Alloy disorder limited mobility of InGaN two-dimensional electron gas

P. Sohi, J.-F. Carlin, and N. Grandjean

Alloy disorder limited mobility of InGaN two-dimensional electron gas

P. Sohi,[a] J.-F. Carlin, and N. Grandjean

Institute of Physics, École Polytechnique Fédérale de Lausanne (EPFL), CH-1015 Lausanne, Switzerland

The mobility of an InGaN based two-dimensional electron gas is determined for an indium content ranging from 0 to 20%. While the electron density remains constant at $\sim 2.5 \times 10^{13}\,cm^{-2}$, the room-temperature mobility drastically decreases from 1340 to 173 $cm^2\ V^{-1}\ s^{-1}$ as the In content increases. In fact, the mobility already drops below 600 $cm^2\ V^{-1}\ s^{-1}$ for an In content as low as 3%. A theoretical model including random alloy fluctuations reproduces well the experimental data confirming that alloy disorder is the main scattering mechanism. With the aim of probing how sensitive the electron mobility is to the InGaN channel/barrier interface, a very thin GaN interlayer was inserted. A dramatic increase in the mobility is observed even for 2 nm of GaN, shedding light on the impact of unintentional GaN interlayers, which may form upon growth conditions or reactor-associated parasitic deposition. © *2018 Author(s). All article content, except where otherwise noted, is licensed under a Creative Commons Attribution (CC BY) license (http://creativecommons.org/ licenses/by/4.0/).* https://doi.org/10.1063/1.5030992

InN and its alloys formed with GaN and AlN have been recently receiving considerable attention in the field of high frequency and high power electronics.[1,2] For instance, lattice-matched InAlN/GaN heterostructures have enabled two-dimensional electron gases (2DEGs) with high carrier densities $(2.6 \times 10^{13}\,cm^{-2})$,[3,4] while keeping the barrier thickness below 10 nm, a key device parameter for achieving high frequency operation.[5,6] The high electron saturation velocity of InN[7] and its large piezoelectric polarization-mismatch to GaN[8] suggest that In-rich InGaN alloys could be of interest as channel materials, giving rise to even higher frequency/power device performance. Moreover, the much smaller electron effective mass of InN (0.05 m_0)[8] compared to GaN (0.2 m_0)[8] should theoretically lead to higher electron mobilities. On the other hand, compared to other III-V semiconductors, III-nitrides exhibit a much larger effective mass, which in turn leads to huge alloy scattering (e.g., 30 times stronger than in III-arsenides). It is therefore of interest to determine the dominating scattering mechanism limiting the electron mobility in In-rich InGaN 2DEGs. Over the past decade, several groups have reported on the electronic properties of 2DEGs based on InGaN channels[9–26] with mobilities exceeding by far those measured in In-rich InGaN bulk alloys. For instance, a mobility of 1240 $cm^2\ V^{-1}\ s^{-1}$ was measured for an $In_{0.1}Ga_{0.9}N$ 2DEG[24] compared to 227 $cm^2\ V^{-1}\ s^{-1}$ in the bulk.[27] At first sight, this might be surprising if one considers that the mobility of a 2DEG is affected by the presence of additional scattering mechanisms such as high carrier density and interface roughness. Another issue when dealing with 2DEG heterostructures featuring InGaN channels is the growth of In-rich InGaN layers, which is challenging due to the high vapor pressure of InN and the large lattice-mismatch to GaN.[28] This may lead to strain relaxation, poor crystal quality, and rough surface morphology, which eventually should impact the transport properties. The difficulty associated with the growth of InGaN alloys can explain the highly dispersed electron mobility data measured for 2DEG InGaN based heterostructures, which span from 300 to 1240 $cm^2\ V^{-1}\ s^{-1}$ for $x = 0.1$.[17,24]

In this study, we determine the electron mobility of 2DEGs in $In_xGa_{1-x}N$ channels for In contents ranging from 0 to 20%. The room-temperature mobility drops from 1340 for a pure GaN channel to 565 $cm^2\ V^{-1}\ s^{-1}$ for an In content as low as 2.8%. A model accounting for alloy scattering reproduces well the data. Furthermore, we demonstrate how the presence of a very thin GaN interlayer (a few nm thick) between the InGaN channel and the barrier can lead to high electron mobility.

Samples used in this study were grown on 2 in. *c*-plane sapphire substrates by metal-organic vapor phase epitaxy (MOVPE) in a horizontal AIXTRON 200/4 RF-S reactor. The absence of a shower head eliminates a potential parasitic source of Ga that could give rise to unintentional GaN interlayers between the channel and the barrier when switching from InGaN to AlN or AlGaN barrier materials.[29–33] The group-III precursors were trimethylgallium, triethylgallium, trimethylaluminum and trimethylindium, for which we used N_2 and H_2 as carrier gases. Each growth started with substrate annealing at 1200 °C under H_2 and NH_3, followed by a low temperature (750 °C) AlN nucleation layer (70 nm) and a 2 μm undoped GaN buffer at 950 °C. InGaN channels of 5 nm thickness were grown in a temperature range between 740 and 900 °C depending on the In content. The 2DEG heterostructure consists of a 5 nm InGaN channel, a 1 nm AlN spacer, a 10 nm $In_{0.18}Al_{0.82}N$ barrier, and a 2 nm GaN cap. The barrier was grown at low temperatures (800 °C) in order to avoid In desorption and interdiffusion. A Brucker New D8 Discovery high-resolution X-ray diffraction (HR-XRD) system was used for (0002) $2\theta–\omega$ diffraction and reflectivity measurements. X-ray reflectivity allowed us to exclude the presence of unintentional GaN interlayers between the channel and the barrier within an accuracy of 1 nm. The layer thickness and the In content were determined by fitting the

a)pirouz.sohi@epfl.ch

XRD and reflectivity curves. The uncertainties in the fitting procedure are expressed as error bars for all samples. We also performed low temperature (11 K) photoluminescence (PL) measurements (He-Cd laser, $\lambda_{\text{ext.}} = 325$ nm, $P = 4.9$ W cm^{-2}) to get additional insights into the InGaN channel properties. The electron mobility of InGaN channels was measured by the Hall effect on 5×5 mm^2 van der Pauw geometry structures at room temperature.

We first prepared a series of samples consisting of 5 nm thick In$_x$Ga$_{1-x}$N channels pseudomorphic to GaN with the In content ranging from 0 to 20%, as deduced by HR-XRD. Low-temperature PL measurements provide qualitative information regarding InGaN alloy disorder. As displayed in Fig. 1, the emission energy peak clearly decreases from 3.49 eV, for a pure GaN channel to 1.98 eV for In$_{0.2}$Ga$_{0.8}$N. This large redshift of the PL energy is the consequence of the built-in electric field present in the 5 nm InGaN channel, which gives rise to a giant quantum confined Stark effect. Another striking feature is the increase in the full width at half maximum (FWHM) of the PL peak from about 20 to 340 meV for GaN and In$_{0.2}$Ga$_{0.8}$N, respectively. The origin of this broadening is twofold: (i) the increase in the InGaN alloy disorder and (ii) the increase in the internal electric field combined with the InGaN channel thickness variations. Notice that the additional features that appear on the broad PL spectra are due to Fabry-Perot interference. Interestingly, the PL broadening experiences a steep increase when the In content reaches 5%. One could thus expect a related decrease in the 2DEG mobility, even for such low In content.

The room-temperature electron mobility of InGaN channel based heterostructures was measured as a function of In content (dark blue squares in Fig. 2). The mobility drastically decreases from 1340 to 173 cm^2 V^{-1} s^{-1} when the In content varies from 0 to 20%, while the electron density remains constant at $n = 2.47 \times 10^{13}$ cm^{-2} (supplementary material). Interestingly, the mobility drops drastically even for a very low In composition, e.g., 2.8%. Actually, theoretical calculations based on the localization landscape theory reported by Piccardo et al.[34] demonstrate that even a few % indium lead to significant fluctuations of the conduction band potential. This is also in line with our recent investigations on InGaN absorption edge broadening, which shows a significant
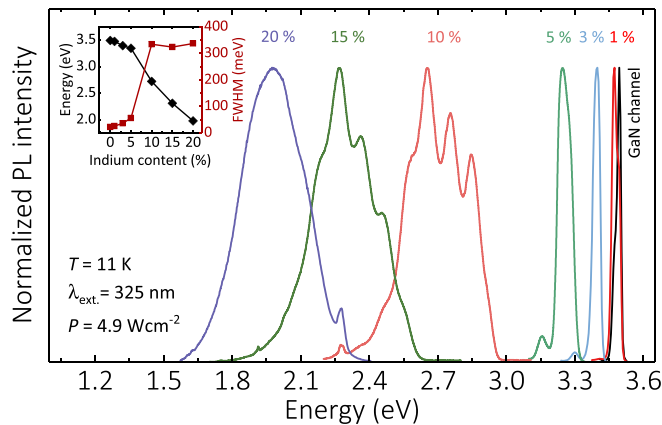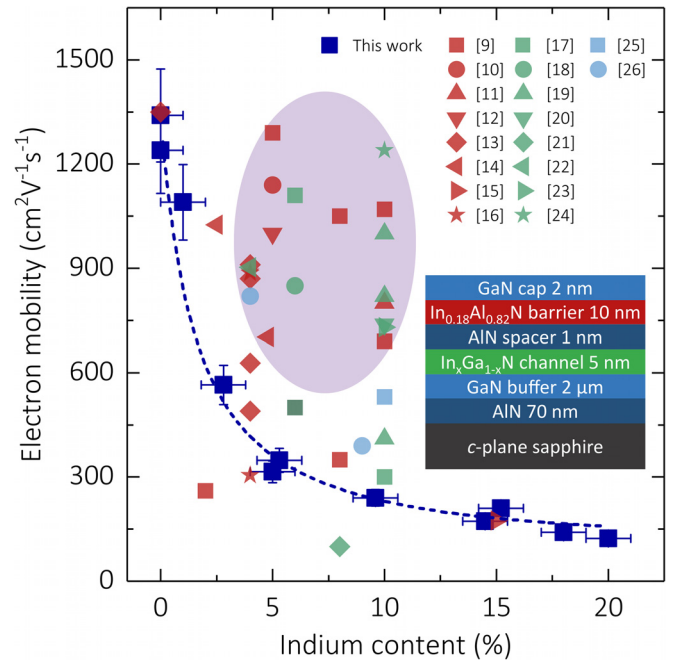

FIG. 2. Electron mobility of the In$_x$Ga$_{1-x}$N channel as a function of In content (dark blue squares). The dashed blue curve shows the theoretical mobility including alloy scattering. Red, green, and light blue data points represent values from the literature. The purple shaded area shows mobility values that are far higher than what is expected from alloy scattering theory. Inset: Sample structure of the present study.

increase in the alloy disorder for In content exceeding 2%.[35] Another peculiar feature is that the mobility somehow staggers for high In content ($x \geq 0.15$), which is consistent with saturation of the alloy disorder potential fluctuations.[34] To get a deeper insight into the scattering mechanisms responsible for the mobility decrease, we developed a simple model accounting for alloy disorder. Due to the high vapor pressure of InN, In-rich layers require low growth temperatures, which in turn result in low adatom mobility and hence a rough surface morphology. Since the 2DEG is separated from the InAlN barrier by an AlN spacer, we consider the alloy disorder scattering contribution as coming only from the InGaN channel. Equation (1) describes the alloy scattering term[36] of the mobility, where m is the linearly interpolated electron effective mass of In$_x$Ga$_{1-x}$N, Ω is the wurtzite unit cell volume $(\sqrt{3}/2a^2c)$ with a and c being the interpolated In$_x$Ga$_{1-x}$N lattice constants and δV is the alloy fluctuation potential, which is assumed to be close to the conduction-band offset between GaN and InN.[36] κ is the wave vector, characterizing the extent of the electron wave function in the alloy, which we estimated from the FWHM of the electron density from Schrödinger-Poisson calculations (see supplementary material)[37]

$$\frac{1}{\mu_{\text{Alloy}}} = \frac{m^2 \Omega \delta V^2 x(1-x)\kappa}{2e\,\hbar^3}. \tag{1}$$

Applying Matthiessen's rule, by combining the alloy scattering term with the experimentally determined mobility of In$_x$Ga$_{1-x}$N at $x = 0$ (which incorporates all other scattering mechanisms), the total mobility can be expressed as a function of indium content (dashed line in Fig. 2). There is a

FIG. 1. Low temperature photoluminescence spectra of In$_x$Ga$_{1-x}$N channels as a function of In content. (Inset) Emission energy and FWHM.

good agreement between our experimental data and the theoretical mobility values for an alloy fluctuation potential of 2.4 eV, which corresponds to the conduction-band offset between GaN and InN reported by van de Walle and Neugebauer.[38] Recently, more rigorous theoretical calculations based on Monte-Carlo simulations also predicted that the electron mobility of InGaN channels is strongly reduced by alloy disorder.[39]

In Fig. 2, we also display experimental mobilities measured in InGaN based 2DEGs, as reported in the literature for a wide variety of barriers (AlGaN,[11,17–21,23,25] InAlN,[12,14,16,22,26] and InAlGaN[9,10,13,24]) and channel thicknesses. Many of these values (shaded area in Fig. 2) are much higher than what is expected from alloy scattering theory. The large data scattering is a strong argument in favor of an extrinsic origin for high electron mobility in InGaN channels. We thus suspect that growth issues might be involved such as: (i) the use of a too high growth temperature for the barrier, which may induce In desorption during the temperature ramp and (ii) residual Ga atoms present in the growth chamber, particularly from the shower head in vertical MOVPE reactors, resulting in the parasitic growth of unintentional GaN layers between the InGaN channel and the barrier.

The impact of thin GaN interlayers on the electron mobility of InGaN channels was first numerically investigated for the In content of 15%. Schrödinger-Poisson calculations were performed in order to elucidate how the electron density distribution of the 2DEG evolves as a function of GaN interlayer thickness. The conduction band profile and the electron density are reported in Fig. 3. In the absence of a GaN interlayer (black curve), the 2DEG is fully confined within the InGaN channel, and hence subjected to alloy disorder scattering. For 3 and 6 nm thick GaN interlayers (red and blue curves, respectively), the electron density exhibits two maxima, one located in the GaN interlayer itself and the other in the InGaN channel. One can also see that the electron density of the InGaN layer decreases to the benefit of the GaN interlayer when increasing the GaN thickness. The electron mobility of such a system should depend on the relative electron distribution over the GaN and InGaN layers. Let us define p_{GaN} and p_{InGaN} as the probability of an electron to be in the GaN or InGaN layer. Those probabilities are
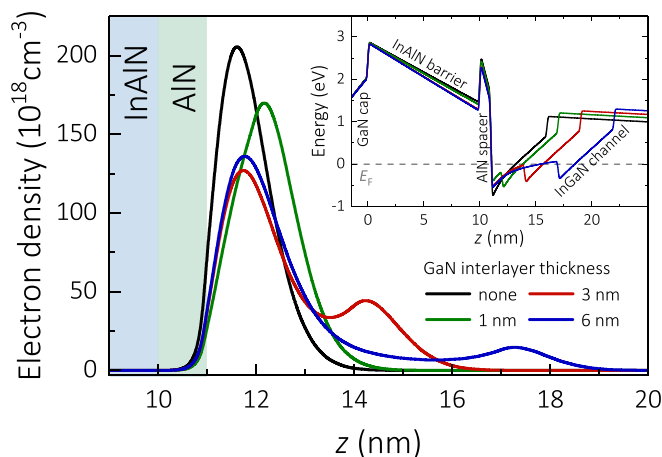
calculated by integrating the electron density over the GaN and InGaN regions, respectively. The electron mobility is then given by Eq. (2), where μ_{GaN} and μ_{InGaN} are the experimental mobilities of GaN and $In_{0.15}Ga_{0.85}N$, respectively (taken from Fig. 2),

$$\frac{1}{\mu} = \frac{p_{GaN}}{\mu_{GaN}} + \frac{p_{InGaN}}{\mu_{InGaN}}. \tag{2}$$

The calculated mobility as a function of the GaN interlayer thickness is shown in Fig. 4 (dashed curve). We observe a strong increase in the mobility when the GaN interlayer thickness gets only a few nanometer thick.

In order to experimentally confirm our findings, we grew a series of 2DEG heterostructures consisting of an $In_{0.15}Ga_{0.85}N$ channel with intentionally grown thin GaN interlayers under the same growth conditions. The In content of the channel was confirmed by HR-XRD to be $15 \pm 1\%$ for all samples. The evolution of 2DEG mobility as a function of GaN thickness is displayed in Fig. 4 (blue diamonds). The electron density remained nearly constant (2.4×10^{13} cm^{-2}) (supplementary material). The experimental data agree well with the calculated values. Figure 4 shows that a very thin GaN interlayer (a few nanometer thick) can dramatically affect the 2DEG mobility in InGaN based channel heterostructures. Another important conclusion can be drawn from Fig. 4, which is that the dominating scattering mechanism is the alloy disorder and not the interface roughness. Indeed, if the mobility of $In_xGa_{1-x}N$ channels with high In content ($x \geq 0.15$) was limited by interface roughness, a thin GaN interlayer grown at low temperatures (800 °C) would not markedly improve the surface morphology, and therefore would not help in recovering the mobility.

In summary, we determined the electron mobility of InGaN based 2DEGs for an In content ranging from 0 to
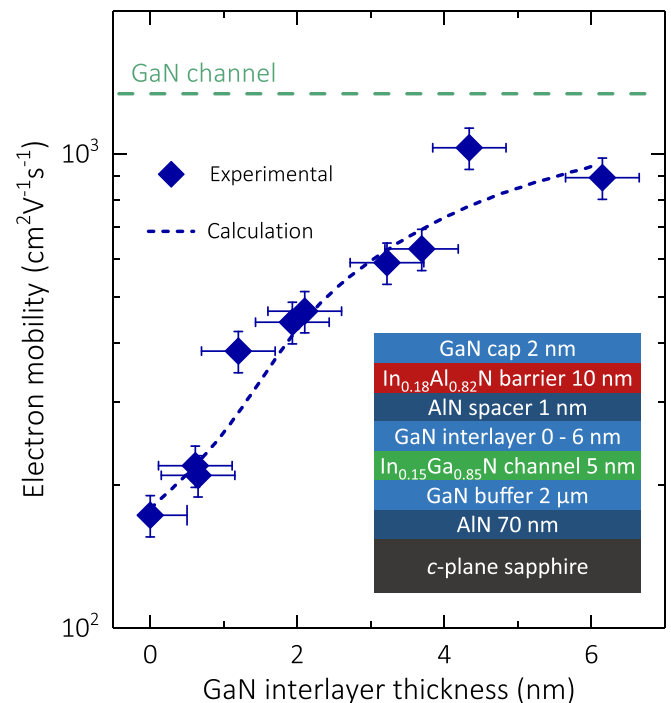
FIG. 3. Electron density distribution of the $In_{0.15}Ga_{0.85}N$ channel as a function of GaN interlayer thickness. Inset: Conduction band profile.

FIG. 4. Electron mobility of the $In_{0.15}Ga_{0.85}N$ channel as a function of GaN interlayer thickness (blue diamonds). The dashed blue curve shows the calculated mobility. Inset: Sample structure.

20%. We observe a strong decrease in the mobility with increasing In content, which we ascribe to alloy disorder scattering. The data are reproduced well by a model taking into account an alloy fluctuation potential, corresponding to the conduction-band offset between InN and GaN.[38] The dramatic decrease in the mobility with increasing In composition furthermore shows that not only holes but also electrons are strongly affected by alloy disorder, which is in line with recent theoretical studies based on the localization landscape theory.[34] Finally, we demonstrated that a very thin GaN interlayer gives rise to high mobility due to the redistribution of electrons from the InGaN channel to the GaN interlayer, even for a few nanometers of GaN.

See supplementary material for the description of: (A) the theoretical estimation of the 2DEG wave vector κ as a function of In content and (B) the experimentally determined electron density as a function of In content and GaN interlayer thickness.

[1]M. Singh and J. Singh, J. Appl. Phys. **94**, 2498 (2003).

[2]T. Palacios, Phys. Status Solidi A **206**, 1145 (2009).

[3]J. Kuzmík, IEEE Electron Device Lett. **22**, 510 (2001).

[4]M. Gonschorek, J.-F. Carlin, E. Feltin, M. A. Py, and N. Grandjean, Appl. Phys. Lett. **89**, 062106 (2006).

[5]D. S. Lee, X. Gao, S. Guo, D. Kopp, P. Fay, and T. Palacios, IEEE Electron Device Lett. **32**, 1525 (2011).

[6]Y. Yue, Z. Hu, J. Guo, B. Sensale-Rodriguez, G. Li, R. Wang, F. Faria, T. Fang, B. Song, X. Gao, S. Guo, T. Kosel, G. Snider, P. Fay, D. Jena, and H. Xing, IEEE Electron Device Lett. **33**, 988 (2012).

[7]B. E. Foutz, S. K. O'Leary, M. S. Shur, and L. F. Eastman, J. Appl. Phys. **85**, 7727 (1999).

[8]C. Wood and D. Jena, *Polarization Effects in Semiconductors: From Ab Initio Theory to Device Applications* (Springer Science & Business Media, New York, 2008).

[9]O. Laboutin, Y. Cao, W. Johnson, R. Wang, G. Li, D. Jena, and H. Xing, Appl. Phys. Lett. **100**, 121909 (2012).

[10]R. Wang, G. Li, G. Karbasian, J. Guo, F. Faria, Z. Hu, Y. Yue, J. Verma, O. Laboutin, Y. Cao, W. Johnson, G. Snider, P. Fay, D. Jena, and H. Xing, Appl. Phys. Express **6**, 016503 (2013).

[11]N. Pala, S. Rumyantsev, M. Shur, R. Gaska, X. Hu, J. Yang, G. Simin, and M. A. Khan, Solid-State Electron. **47**, 1099 (2003).

[12]Y. Zhang, Z. Wang, S. Xu, D. Chen, W. Bao, J. Zhang, J. Zhang, and Y. Hao, Appl. Phys. Lett. **111**, 222107 (2017).

[13]J. Xie, J. H. Leach, X. Ni, M. Wu, R. Shimada, Ü. Özgür, and H. Morkoç, Appl. Phys. Lett. **91**, 262102 (2007).

[14]Y. Zhang, X. Zhou, S. Xu, Z. Wang, Z. Chen, J. Zhang, J. Zhang, and Y. Hao, AIP Adv. **5**, 127102 (2015).

[15]Y. M. Hsin, H. T. Hsu, C. C. Chuo, and J. I. Chyi, IEEE Electron Device Lett. **22**, 501 (2001).

[16]Y. Zhang, X. Zhou, S. Xu, Z. Wang, Y. Zhao, J. Zhang, D. Chen, J. Zhang, and Y. Hao, Appl. Phys. Lett. **106**, 152101 (2015).

[17]N. Okamoto, K. Hoshino, N. Hara, M. Takikawa, and Y. Arakawa, J. Crystal Growth **272**, 278 (2004).

[18]N. Maeda, T. Saitoh, K. Tsubaki, T. Nishida, and N. Kobayashi, Jpn. J. Appl. Phys. Lett., Part 2 **38**, L799 (1999).

[19]C. X. Wang, K. Tsubaki, N. Kobayashi, T. Makimoto, and N. Maeda, Appl. Phys. Lett. **84**, 2313 (2004).

[20]G. Simin, X. Hu, A. Tarakji, J. Zhang, A. Koudymov, S. Saygi, J. Yang, A. Khan, M. S. Shur, and R. Gaska, Jpn. J. Appl. Phys. **40**, L1142 (2001).

[21]H. Ikki, Y. Isobe, D. Iida, M. Iwaya, T. Takeuchi, S. Kamiyama, I. Akasaki, H. Amano, A. Bandoh, and T. Udagawa, Phys. Status Solidi A **208**, 1614 (2011).

[22]S. Gökden, R. Tülek, A. Teke, J. H. Leach, Q. Fan, J. Xie, Ü. Özgür, H. Morkoç, S. B. Lisesivdin, and E. Özbay, Semicond. Sci. Technol. **25**, 045024 (2010).

[23]G. Simin, A. Koudymov, H. Fatima, J. Zhang, J. Yang, M. A. Khan, X. Hu, A. Tarakji, R. Gaska, and M. S. Shur, IEEE Electron Device Lett. **23**, 458 (2002).

[24]V. Adivarahan, M. E. Gaevski, M. M. Islam, B. Zhang, Y. Deng, and M. A. Khan, IEEE Trans. Electron Devices **55**, 495 (2008).

[25]R. L. Wang, Y. K. Su, and K. Y. Chen, Electron. Lett. **42**, 718 (2006).

[26]J. Liberis, I. Matulioniene, A. Matulionis, E. Sermuksnis, J. Xie, J. H. Leach, and H. Morkoç, Phys. Status Solidi A **206**, 1385 (2009).

[27]C. Wang, N. Maeda, K. Tsubaki, N. Kobayashi, and T. Makimoto, Jpn. J. Appl. Phys. **43**, 3356 (2004).

[28]H. Morkoç, *Handbook of Nitride Semiconductors and Devices* (Wiley-VCH, Weinheim, 2009), Vol. 1.

[29]S. Choi, H. J. Kim, Z. Lochner, J. Kim, R. D. Dupuis, A. M. Fischer, R. Juday, Y. Huang, T. Li, J. Y. Huang, F. A. Ponce, and J. H. Ryou, J. Crystal Growth **388**, 137 (2014).

[30]J. Kim, Z. Lochner, M. H. Ji, S. Choi, H. J. Kim, J. S. Kim, R. D. Dupuis, A. M. Fischer, R. Juday, Y. Huang, T. Li, J. Y. Huang, F. A. Ponce, and J. H. Ryou, J. Crystal Growth **388**, 143 (2014).

[31]G. Naresh-Kumar, A. Vilalta-Clemente, S. Pandey, D. Skuridina, H. Behmenburg, P. Gamarra, G. Patriarche, I. Vickridge, M. A. Di Forte-Poisson, P. Vogt, M. Kneissl, M. Morales, P. Ruterana, A. Cavallini, D. Cavalcoli, C. Giesen, M. Heuken, and C. Trager-Cowan, AIP Adv. **4**, 127101 (2014).

[32]J. Kim, M. H. Ji, T. Detchprohm, R. D. Dupuis, A. M. Fischer, F. A. Ponce, and J. H. Ryou, J. Appl. Phys. **118**, 125303 (2015).

[33]M. Hiroki, Y. Oda, N. Watanabe, N. Maeda, H. Yokoyama, K. Kumakura, and H. Yamamoto, J. Crystal Growth **382**, 36 (2013).

[34]M. Piccardo, C. K. Li, Y. R. Wu, J. S. Speck, B. Bonef, R. M. Farrell, M. Filoche, L. Martinelli, J. Peretti, and C. Weisbuch, Phys. Rev. B **95**, 144205 (2017).

[35]R. Butté, L. Lahourcade, T. K. Uzdavinys, G. Callsen, M. Mensi, M. Glauser, G. Rossbach, D. Martin, J.-F. Carlin, S. Marcinkevičius, and N. Grandjean, Appl. Phys. Lett. **112**, 032106 (2018).

[36]G. Bastard, *Wave Mechanics Applied to Semiconductor Heterostructures* (Editions de Physique, Les Ulis, 1990) pp. 219–223.

[37]See www.nextnano.de for semiconductor device simulation software.

[38]C. G. Van de Walle and J. Neugebauer, Nature **423**, 626 (2003).

[39]T. Hoshino and N. Mori, Jpn. J. Appl. Phys. **57**, 04FG06 (2018).